BRAIN CONNECTIVITY
Volume 1, Number 2, 2011

DOI: 10.1089/brain.2011.0014

Broadband Local Field Potentials Correlate with Spontaneous Fluctuations in Functional Magnetic Resonance Imaging Signals in the Rat Somatosensory Cortex Under Isoflurane Anesthesia

Wen-Ju Pan,[1] Garth Thompson,[1] Matthew Magnuson,[1] Waqas Majeed,[1] Dieter Jaeger,[2] and Shella Keilholz[1]

Abstract

Resting-state functional magnetic resonance imaging (fMRI) is widely used for exploring spontaneous brain activity and large-scale networks; however, the neural processes underlying the observed resting-state fMRI signals are not fully understood. To investigate the neural correlates of spontaneous low-frequency fMRI fluctuations and functional connectivity, we developed a rat model of simultaneous fMRI and multiple-site intracortical neural recordings. This allowed a direct comparison to be made between the spontaneous signals and interhemispheric connectivity measured with the two modalities. Results show that low-frequency blood oxygen level-dependent (BOLD) fluctuations (< 0.1 Hz) correlate significantly with slow power modulations (< 0.1 Hz) of local field potentials (LFPs) in a broad frequency range (1–100 Hz) under isoflurane anesthesia (1%–1.8%). Peak correlation occurred between neural and hemodynamic activity when the BOLD signal was delayed by ~4 sec relative to the LFP signal. The spatial location and extent of correlation was highly reproducible across studies, with the maximum correlation localized to a small area surrounding the site of microelectrode recording and to the homologous area in the contralateral hemisphere for most rats. Interhemispheric connectivity was calculated using BOLD correlation and band-limited LFP (1–4, 4–8, 8–14, 14–25, 25–40, and 40–100 Hz) coherence. Significant coherence was observed for the slow power changes of all LFP frequency bands as well as in the low-frequency BOLD data. A preliminary investigation of the effect of anesthesia on interhemispheric connectivity indicates that coherence in the high-frequency LFP bands declines with increasing doses of isoflurane, whereas coherence in the low-frequency LFP bands and the BOLD signal increases. These findings suggest that resting-state fMRI signals might be a reflection of broadband LFP power modulation, at least in isoflurane-anesthetized rats.

Key words: anesthetic effects; broadband LFP; functional connectivity; neural correlates; resting-state fMRI

Introduction

Functional magnetic resonance imaging (fMRI) is an important tool for exploring brain function that provides significant advantages over traditional recording techniques, including the ability to noninvasively measure functional activity of large-scale brain networks. Because fMRI measures a surrogate signal of neural activity, the blood oxygen level-dependent (BOLD) signal, as opposed to measuring neuronal activity directly, the correspondence between BOLD and neural activity is not straightforward. Neural recording methods such as extracellular local field potential (LFP) measurements, on the other hand, directly detect the electrical activity in the brain. However, these techniques are highly invasive and are typically limited to a few targeted areas. Combining the merits of fMRI and electrophysiological recording may therefore provide an enhanced tool for examining network activity in the brain and could potentially lead to a better understanding of brain function (Logothetis, 2008).

To date, only a few laboratories have successfully measured fMRI BOLD signals and intracortical neural activity simultaneously due to the technical challenges involved in combining the experiments, but the results from these studies have provided some of the most important insights into the relationship between BOLD and neural activity (Huttunen et al., 2008; Logothetis et al., 2001; Shmuel and Leopold,

[1]Department of Biomedical Engineering, Emory University/Georgia Institute of Technology, Atlanta, Georgia.
[2]Department of Biology, Emory University, Atlanta, Georgia.

2008). For example, simultaneous fMRI and intracortical recordings in the monkey visual cortex revealed a tight link between the BOLD response and evoked LFPs as compared to multiple/single unit activity (Goense and Logothetis, 2008; Logothetis et al., 2001). Strong coupling between stimulus-elicited LFPs and local tissue oxygen concentration was consistently observed even in the absence of spikes, which confirmed that BOLD signals in fMRI reflect synaptic activity more than spiking rate (Viswanathan and Freeman, 2007).

While the neural correlates of stimulus-induced fMRI activity have been examined, the neural correlates of spontaneous BOLD fluctuations in resting-state fMRI have not been fully explored. The first report on this subject by Shmuel and Leopold found a relationship between the BOLD fluctuations and low-frequency modulation of gamma/multiple unit activity power in the monkey (Shmuel and Leopold, 2008), but the data used were acquired for a stimulus-based experiment and was sub-optimal for the resting-state study (Logothetis et al., 2009). Correlation between spontaneous BOLD fluctuations from different areas of the brain is presumed to reflect functional connectivity and has been reported in several networks (Fox and Raichle, 2007). Recently, a few studies, combining separate experimental sessions of electrophysiology and fMRI, have focused on the neural processes underlying these BOLD signal correlations. Nir et al. (2008) observed high coherence in the power fluctuations of gamma band activity across hemispheres of human auditory system. Lu et al. (2007) reported high delta power coherence in rat somatosensory cortex that decreased in the same manner as BOLD signal correlations with progressively deeper doses of alpha-chloralose. He et al. (2008) have performed separate experiments in presurgical patients using fMRI and multi-site electrocorticography (ECoG), and the slow cortical potentials (<4 Hz) demonstrated a correlation structure similar to that of spontaneous BOLD fluctuations across wakefulness, slow-wave sleep, and rapid-eye-movement sleep. Schölvinck et al. (2010) have recently reported tight coupling of gamma power in a cortical site with global BOLD fluctuation in monkey brain. The variety of the frequency relationships reported, while strongly supporting a neural origin for spontaneous BOLD fluctuations, suggests that the relationship may be state dependent or influenced by experimental limitations. Simultaneous multi-site recording and fMRI studies that allow direct comparison of BOLD fluctuations and concurrent neural activity would be a powerful tool to gain greater insight into the relationship between modalities.

We have developed a rat model of simultaneous fMRI imaging and multi-site electrophysiological recording, which allows the direct examination of the neural correlates of fMRI functional connectivity. Using a simple but typical functional network in the rodent, spontaneous LFPs and BOLD were simultaneously recorded from left and right primary somatosensory areas that typically exhibit strong interhemispheric connectivity during the resting state. First of all, we focused on examining the neural sources of the spontaneous BOLD fluctuations, that is, comparing BOLD and LFP signals from an identical cortical site. With the same temporal scale, the low-frequency fluctuations of band-limited LFPs were directly compared to low-frequency fluctuations in the BOLD signal (<0.1 Hz). In this way, the concurrent low-frequency BOLD activity and slow spontaneous LFP events were obtained and the relationship between them was investigated. An additional analysis examined the relationship between functional connectivity and coherent neural activity, that is, direct measurement of interhemispheric correlation in the BOLD signal and coherence in the band-limited LFPs when varying neural spontaneous activity by manipulating anesthesia levels. The primary results showed that the power of LFPs across a large frequency band (1–100 Hz) significantly correlated with the BOLD signal at the microelectrode recording site and in the contralateral cortical site but not in other areas of the brain. In addition, both interhemispheric BOLD correlation and LFP coherence were modulated by anesthesia level. High-frequency (>25 Hz) LFP power coherence decreased as the isoflurane level increased, whereas low-frequency coherence and BOLD correlation increased.

Methods

Microelectrode implantation

All experiments were performed in compliance with NIH guidelines and were approved by the Emory University Institutional Animal Care and Use Committee. Seven Sprague-Dawley rats (male, 200–300 g) were used in this study. All experiments were conducted at roughly the same time of day, with microelectrode implantation performed in the morning followed by simultaneous recording and imaging in the afternoon. The animals were sacrificed at the end of the experiment.

Each rat was anesthetized under 2% isoflurane during surgery. The fur covering the head was removed and the animal was secured into a stereotactic system (Harvard Apparatus). Eye ointment was applied to prevent corneal drying during the multi-hour experiment. Before surgery began, each rat was checked to ensure that there was no withdrawal response to a toe pinch, which indicates an adequate level of anesthesia. Surgery was performed in several steps. First, an incision was made through the skin covering the skull to expose the bone surface. The exposed skull areas included bregma as well as regions over bilateral S1FL (primary somatosensory of forelimb, 4 mm lateral, and 1 mm frontal to bregma) and the regions in front of the lambdoid suture. Any bleeding from the incision over the skull was stopped with a low-temperature cauterizing device. The rat's body temperature was maintained with a heating pad at a slightly reduced body temperature (to $\sim$36°C) to prevent vasodilation that could increase bleeding.

The second surgical step was to prepare a solid pier on the skull bone for the fixation of the electrode shafts in the last step. The pier was located anterior to the lambdoid suture and beside the sagittal suture. A small nylon screw was secured into the skull before applying the dental cement that was used to build a pier with a base size of about $3\times2\times5$ mm^3 (w, l, h). In the third surgical step, a craniotomy was performed. At the bilateral sites of S1FL (4 mm lateral and 1 mm frontal to bregma), a 1–2 mm hole was opened on each side of the midline using a fine-tip dental drill (Omni-Drill35; World Precision Instruments). Drilling was performed while viewing the site through a microscope until the surface of the dura was revealed. Vessels were visually identified on the brain surface, and a small opening in the

dura was cut in an area relatively free from visible vessels using a 27-gauge syringe needle.

The final surgical step involved implantation and fixation of a pair of glass microelectrodes. The microelectrodes were pulled with a micropipette puller from borosilicate pipettes (PE-2, NARISHIGE) to a tip of $\sim 10\,\mu$m diameter. They were filled with artificial cerebrospinal fluid (ACSF), resulting in a 1–5 MΩ impedance measured at 1 KHz. Using dual stereotactic arms, the two electrodes were inserted separately into the cortex, 0.5–1 mm below the brain surface at a 45-degree angle from back to front. The recorded electrical signals were checked before the microelectrodes were fixed into place. A layer of Colgate toothpaste was applied to replace removed skin and muscle over the skull before fixing the electrodes to the pier prepared in the second step. The use of toothpaste helps to reduce the MRI susceptibility artifacts that occur as a result of the interface between the surface of the brain and the surrounding air (Lewin et al., 1995). We tested several laboratory gels and compared them with Colgate toothpaste, but found the latter is best for minimizing artifacts in the T2-weighted brain image. Because any blood pooling, exudation, or air bubbles that occur on the skull's surface as a result of the surgical procedures can also cause MRI artifacts, the exposed brain and skull surfaces were carefully cleaned and prepared before applying toothpaste and fixing the electrodes to ensure high image quality. We initially tested a surgical strategy that involved suturing the skin after the electrodes were fixed, but blood/exudation pooling and bubbles between the skull and scalp occurred frequently, resulting in unexpected artifacts during imaging. After the surgical area was completely prepared, and the electrical signals were satisfactory, the two glass electrode shafts were fixed to the prepared pier using dental cement. A demonstration of the preparation protocol is available in the *Journal of Visualized Experiments* (Pan et al., 2010).

FMRI imaging and simultaneous LFP recording

After the dental cement cured, the animal was transferred to the MRI cradle and the head held fixed using a bite bar and ear bars. Rectal temperature, respiration rate, SPO_2, and cardiac rate were all continuously monitored and maintained within a normal physiological range. A custom-built surface coil (transmit/receive) was positioned over the head, with the electrodes protruding from the center of the coil. An additional arch-shaped hard cover that sits atop the cradle served as a support for fixation of the electrode leads to avoid motion caused by the animal breathing. Chloridized silver wires were dipped into the ACSF inside the microelectrodes and connected to the recording cable for each recording electrode. A chloridized silver wire was also placed under the skin caudal to the incision over the skull to serve as a reference/ground electrode. The recording cables were ~ 5 m long (the amplifier is located outside the magnet room; A-M Systems) and were covered with conductive plastic, which served as a passive shield. The recording parameters were as follows: ×1000 amplified, 0.1 Hz–5 kHz bandpass-filtered, 60 Hz notch-filtered, and 12 kHz sampling rate for analog to digital conversion.

A 9.4 T small animal MRI system (Bruker) was used in our studies. A three-plane scout image was first acquired to position the fMRI scans. To improve the homogeneity of the magnetic field, the volume of interest (6 mm^3) was shimmed using FASTMAP (Gruetter, 1993). Manual shimming adjustment was applied when necessary to improve the field homogeneity of the selected slice. For fMRI studies, a coronal imaging slice was selected, which included bilateral forepaw primary somatosensory areas, in which the glass recording electrodes were implanted. The EPI imaging parameters were FOV, $1.92 \times 1.92\,cm^2$; matrix size, 64×64; in-plane resolution, $0.3 \times 0.3\,mm^2$; slice thickness, 2 mm; TR/TE, 500/15 ms. The simultaneous electrophysiological recording and fMRI imaging lasted 500 sec for each resting-state scan. Resting state scans were collected under several different concentrations of isoflurane, which ranged from 1% to 1.8%. The isoflurane, in a mixture of O_2 and room air, was continuously delivered to the nosecone, allowing for free breathing throughout the experiment. The rat's oxygen saturation, measured with a pulse oximeter, was kept above 98% throughout the data acquisition process. One to four simultaneous LFP and fMRI recordings were conducted for each animal. With the optimized procedure of electrode implantation described above, the potential interferences to image quality were largely avoided. Figure 1 shows an unmodified EPI image with electrodes implanted; there are no distortions or obvious artifacts. Also, the low-frequency BOLD fluctuations and seed-based functional connectivity between hemispheres

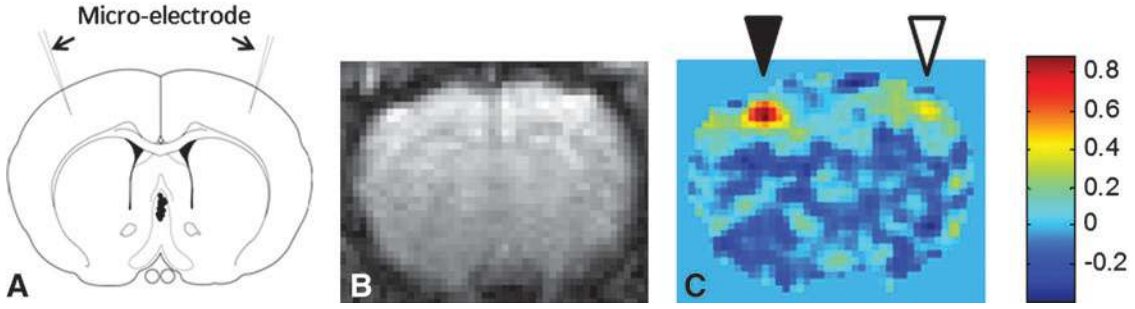

FIG. 1. **(A)** Anatomical schematic showing the location of the implanted electrodes. **(B)** A typical EPI image is shown with two microelectrodes implanted separately in S1FL of left and right hemispheres. There are no obvious artifacts in EPI image due to the electrodes. In traditional seed-based functional connectivity analysis, the seed of S1FL **(**mean time courses from a few voxels in left S1FL, the solid arrow in **C)** correlated significantly with the seed region and the opposite S1FL across hemispheres **(**open arrow in **C)** during the resting state under isoflurane anesthesia. Color bar represents Peason *r*.

were examined, and the results were similar to those previously observed in the intact rat brain (Williams et al., 2010).

Electrophysiological data preprocessing

The raw LFP signal recorded during MRI scanning contained a combination of electrical signals and scanning-related artifacts, which must be removed before further analysis. The offline process of artifact removal was performed in Matlab (Mathworks) and is illustrated in Figure 2. Relative to randomly occurring neural events, the artifact profiles appear at regular intervals and may be extracted by averaging the time courses of all periodic epochs (repetition

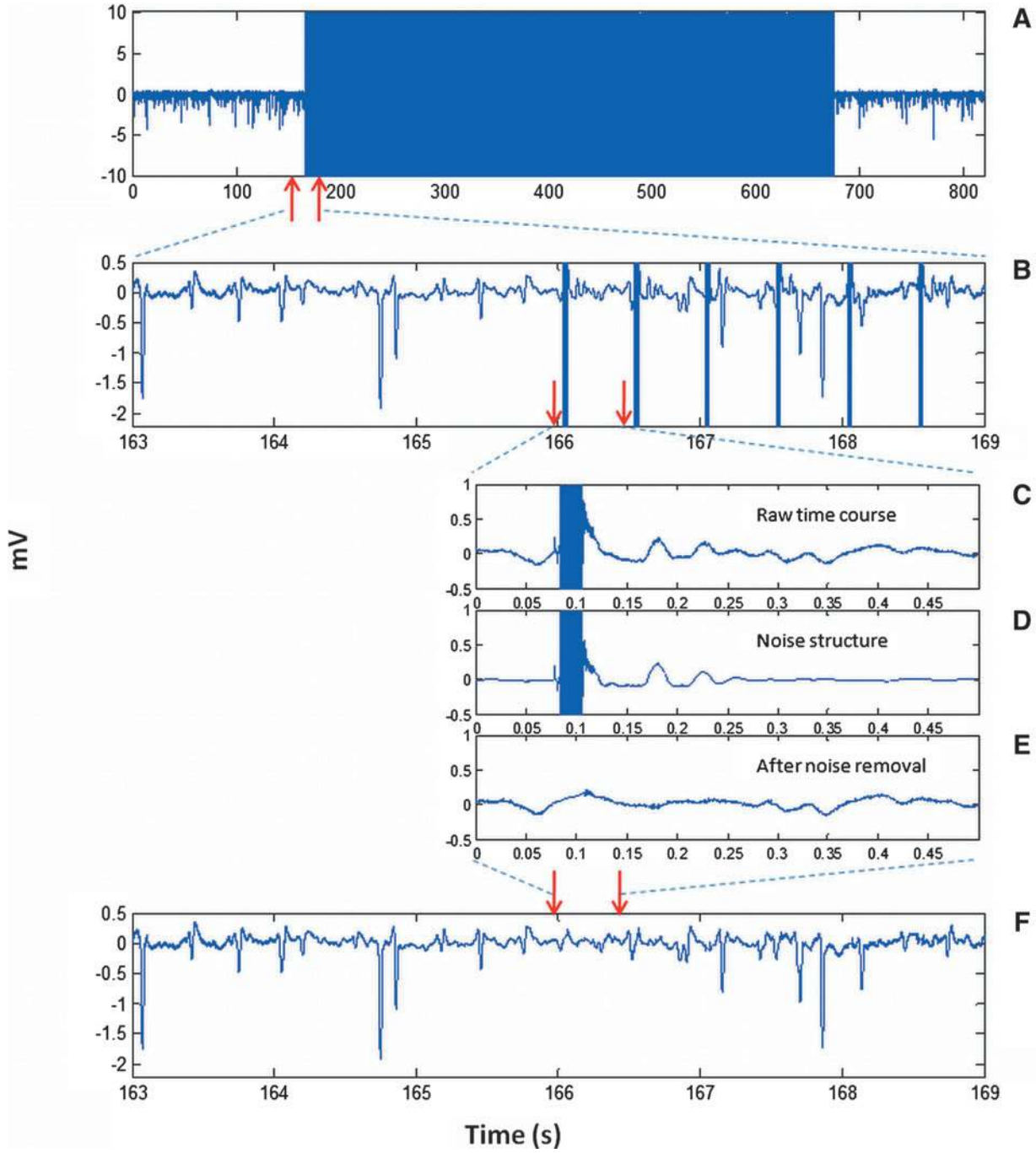

FIG. 2. Illustration of the artifacts in electrophysiological recordings induced by magnetic field alternations during the fMRI scan and artifact removal. The original recording from a typical rat under 1% isoflurane is shown **(A)**, including noisy recordings during fMRI imaging (middle dark section). The major artifacts during scanning (solid bar, seen in **B** and **C**) are saturated recordings due to gradient field switching). The noise structure **(D)** can be extracted by averaging all scan cycles of recordings (one of scan period: between red arrows in **B**). The brief periods of saturation (20 ms of each scan cycle of 500 ms) were refilled with a linear function to maintain continuity **(E)**. After artifact removal, the denoised recordings **(F)** were used for further analysis. fMRI, functional magnetic resonance imaging.

time, TR) in a scanning session (Allen et al., 2000). Artifacts typically consisted of a relatively small signal change caused by RF pulsation, followed by a longer period of large signal fluctuations caused by alternation of the gradients during image acquisition. This gradient-induced artifact, which occupied only a small portion of each scan cycle (<20/500 ms), saturated the amplifier. Each saturated segment was removed and the corresponding time points were filled with values according to a linear function bounded by the two nonsaturated end points before and immediately after image readout. After the cessation of gradient switching, a pattern of nonsaturated decaying oscillations was observed as the signal returned to baseline in ~0.2 sec (Fig. 2D). A template of this nonsaturated portion of the noise structure was created by averaging all TR periods together and then directly subtracted from each time course (Allen et al., 2000). Individual noise epochs were identified by gradient intervals. The noise structure was highly reproducible over time in each experimental session, and not sensitive to neural activity states. For example, in the case of a deeply anesthetized rat (2.5% isoflurane, Fig. 3) in which the neural activity was mostly suppressed and the recorded changes were associated more with scan-related noise rather than neural signals, the extracted noise structures were nearly identical to the noise structures obtained during a scan session using 1% isoflurane (Figs. 3 vs. 2D). The artifact removal algorithm used in the present study therefore indicated that the imaging-related artifacts were extracted independent of the level of neural activity. In this study, the denoised time courses were converted to LFP (1–100 Hz) power time courses, which reflect power modulation of LFP activities (Manning et al., 2009). The windows of nonsaturated segments between TRs (~480 ms; not including the segments affected by removal of gradient artifacts) were used to compute LFP power of >8 Hz frequency components by fast Fourier transform, whereas 2 sec windows were used in computing 1–8 Hz LFP power. The time window was moved in steps of 0.5 sec (TR), which is the same temporal resolution as fMRI. Finally, the power time courses were band-filtered within 0.01–0.1 Hz.

FMRI data preprocessing

Each fMRI scanning session included 1000 single-slice images acquired over 8.3 min. Twenty dummy scans were acquired to reduce transient signal intensity fluctuations at the start of the image series. Data were analyzed using MatLab and SPM 8 (www.fil.ion.ucl.ac.uk/spm). To reduce unnecessary computing, a brain mask was first obtained using a Seed Growth algorithm; the initial pixel was chosen in the brain. In the image matrix, two or more rows/columns outside the brain mask were removed to decrease image size and the time needed to process the data set. Head motion occurring during scanning sessions was corrected in SPM 8. If the brain position shifted more than one pixel across the data acquisition period or if "spike-like" abrupt head motion was observed, the data were not used for further analysis. The images were then smoothed using a Gaussian filter with an FWHM of 0.5 mm in all directions. Linear drift and global signals were removed by regression. Finally, the time series of each voxel in the brain was band-filtered (0.01–0.1 Hz) and normalized to unit variance (percent change) for further statistical analysis.

Correlation analysis between fMRI BOLD and LFPs

The relationship between spontaneous BOLD fluctuations and LFPs was first examined by directly comparing the recorded LFPs from one electrode and the BOLD signal from the surrounding voxels. The frequency-specific power time courses (1–100 Hz) were first calculated in MatLab. LFP power time courses were then normalized to unit variance (percent change) and bandpass filtered at 0.01–0.1 Hz. The Pearson correlation coefficients between these LFP power time courses and the BOLD signal were calculated for time lags from −2.5 to 9.5 sec (BOLD relative to LFPs, 0.5-sec step). This range is roughly symmetric around the expected peak correlation at 4 sec due to the previously measured hemodynamic delay in the rat (Martin et al., 2006).

The second analysis compared interhemispheric connectivity between band-limited LFPs and fMRI BOLD signals at different anesthetic depths. Under isoflurane anesthesia, the spontaneous neural electrical signals showed general suppression with intervening irregular burst activation (Fig. 4, red arrows), which were modified by altering the anesthetic levels (Vincent et al., 2007). In this study, the effective level of anesthesia was assessed by measuring the suppression period of inter-burst intervals, which were proportionally prolonged during increased isoflurane administration. The average length of the neural suppression period in each session was taken as an index of anesthesia effects on neural

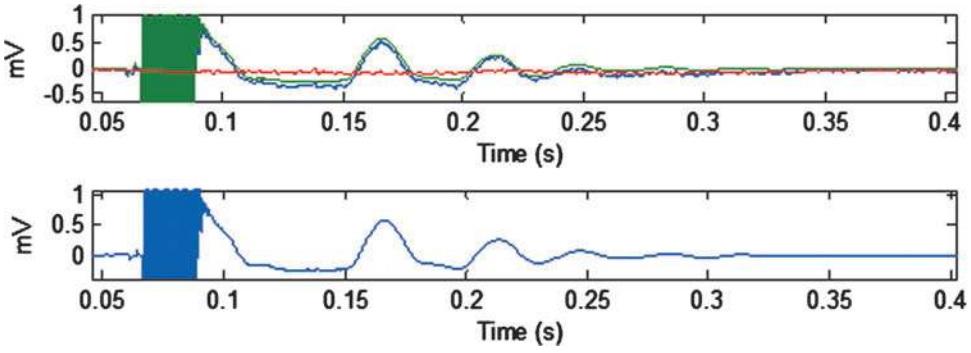

FIG. 3. Similar imaging-induced noise profiles in recordings in the case of absent neural activity. During extremely deep anesthesia (isoflurane >2.5%), the neural spontaneous activity was largely suppressed (red). The noise profile (blue) is similar to the original recording (green) due to the largely absent neural activity. The noise structure appears nearly identical to recordings acquired in a moderately anesthetized state where more neural activity is present (Fig. 2D), and includes three components, an initial brief low-amplitude oscillation induced by the RF coil, a period of saturated oscillations related to rapid switching of the gradient, followed by induced oscillations that gradually attenuated to zero over ~0.2 sec (blue).

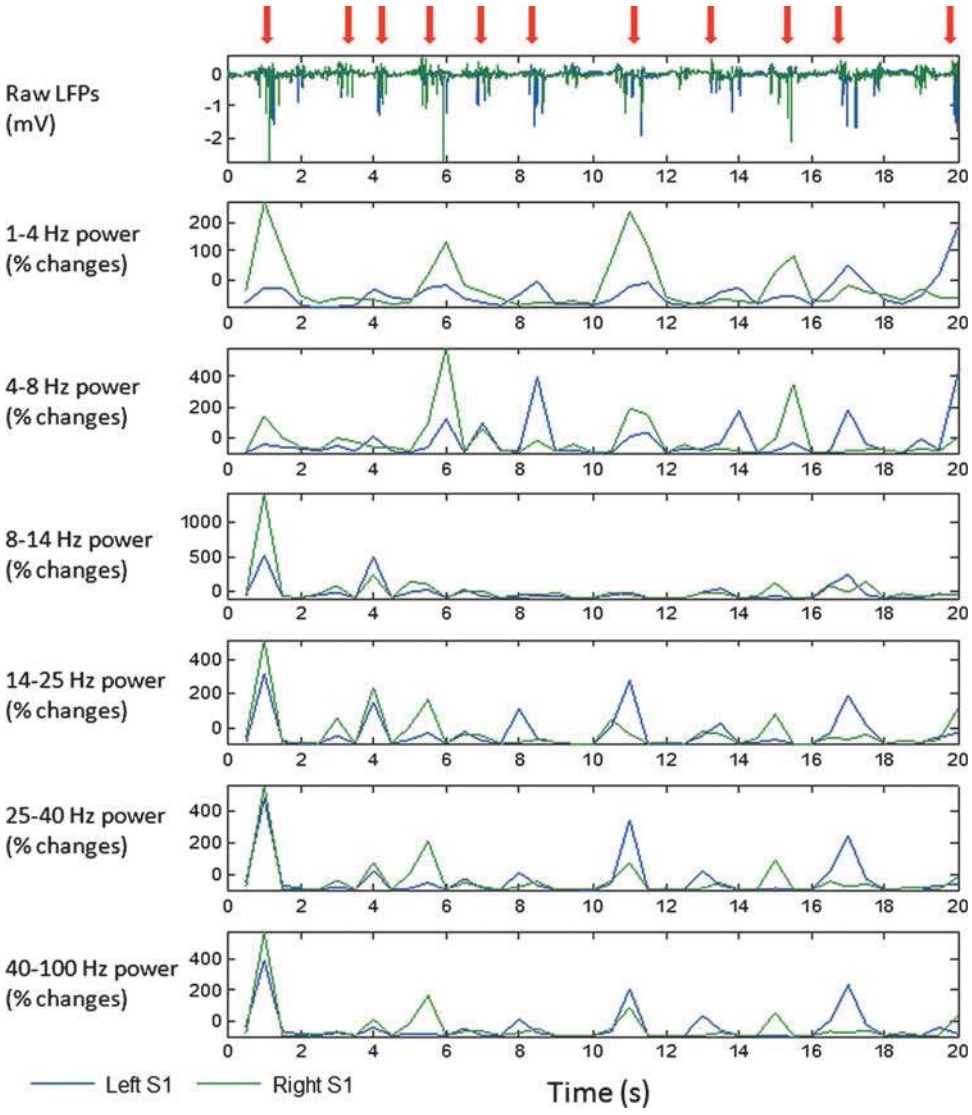

FIG. 4. Synchronized burst activity across hemispheres and spectrum from one rat under 1.5% isoflurane. During isoflurane anesthesia, the neural activity typically showed general suppression with intervening irregular burst activation (red arrow). The bursts of LFP and its power were highly synchronized in SI regions of left (blue) and right (green) hemispheres. The synchronized LFP powers were similar in phase across all LFP frequency bands from 1 to 100 Hz. Correlation between the time courses from each electrode was also calculated for each animal and is shown in Figure 7. LFP, local field potential.

activity (neural suppression index [NSI]). The NSIs for each scanning session were calculated as the total suppression length divided by total time-course length. Suppression periods were identified according to power of LFPs. In LFP power time courses (after normalization by percent change), difference of $<15\%$ between neighboring time points was considered suppression. Correlation between LFPs recorded from opposite hemispheres (separated into 1–4, 4–8, 8–14, 14–25, 25–40, and 25–100 Hz bands) was plotted against NSI. A similar analysis was performed for BOLD signal correlation. Finally, the relationship between BOLD correlation and correlation in each LFP band was examined.

Results

Correlation between BOLD signals and LFPs at a single recording site

Temporal correlation pattern. For most rats, the power time course of LFPs for all frequencies between 1 and 150 Hz exhibited strong correlation with the BOLD signal at the recording site, with correlation persisting throughout the full range of frequencies (1–300 Hz) in some rats. Figure 5A shows the correlation between BOLD and LFP power as a function of frequency and time lag, averaged over all rats. Correlation was strongest for frequencies above 25 Hz and below 150 Hz. The same data are shown for individual scans in Figure 5B, and clearly indicate that a broad range of LFPs correlates with the BOLD signal even in single trials. Correlation as a function of lag time (averaged across all frequencies) is plotted in Figure 5C, and shows that the hemodynamic delay corresponding to peak correlation ranges from $\sim$2 to 6 sec in individual rats, with an average value of $\sim$4 sec. These results clearly indicate that the BOLD signal is related to the power modulation of LFPs in a wide range of frequencies in the isoflurane-anesthetized rat.

Spatial correlation pattern. Using the broadband LFP power time course from one electrode as a seed, the cross-correlation coefficient was calculated between the seed and BOLD time courses from the whole brain on a voxel-by-voxel basis using lags of -2.5 to 9.5 sec (in 0.5 sec intervals) for BOLD relative to LFPs. The resulting correlation maps showed that the highest correlation occurred in the voxels

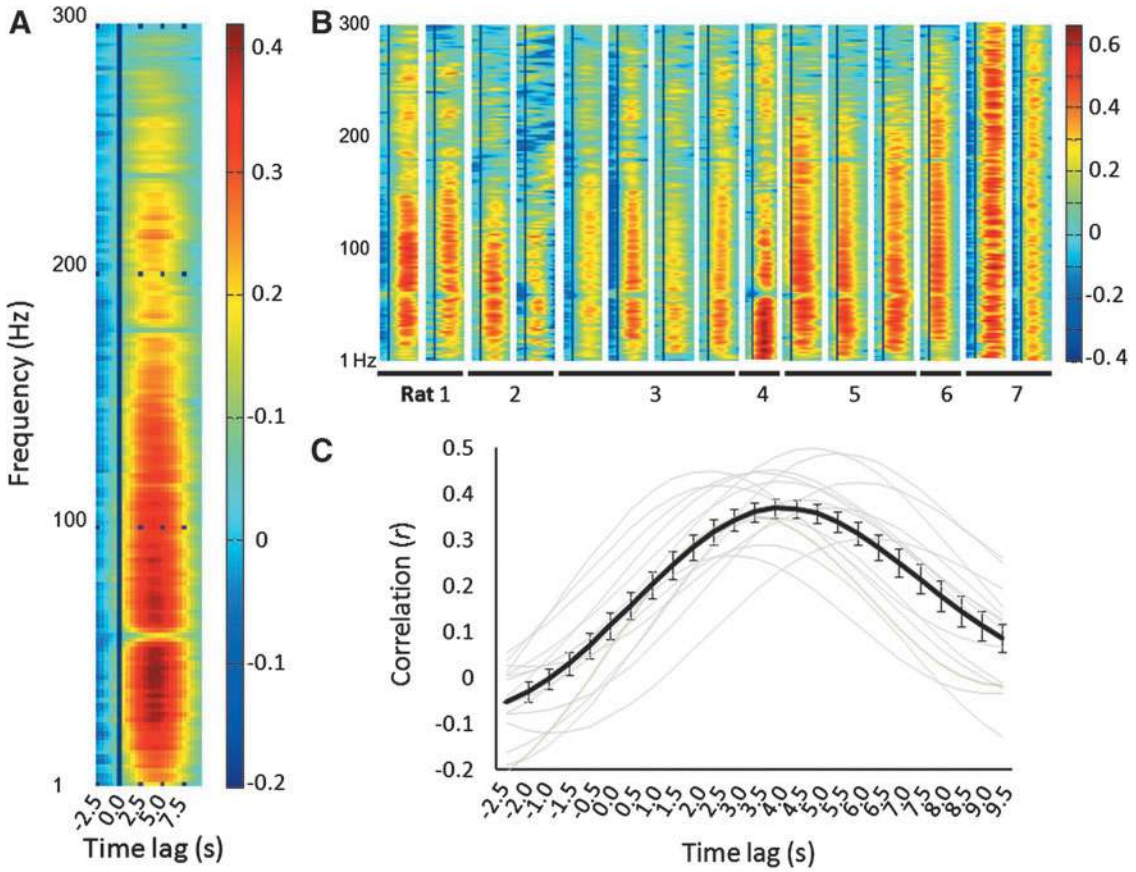

FIG. 5. Correlation analysis between power modulation of LFPs (1–300 Hz) and BOLD at the recording site of interest. The left panel **(A)** shows averaged results from all 15 sessions of 7 rats **(B)**. Strong correlation between the BOLD signal and LFPs is observed across the broad range of frequencies. The strongest correlations for all 15 data sets are below 150 Hz. Due to the use of a notch filter at 60 Hz, the recordings at this frequency were attenuated. **(C)** The mean correlation showed the peak correlation at lags ranging from 2 to 6 sec in the individual data (gray), with the average delay at ~4 sec time lag for BOLD (mean ± standard errors (dark)). BOLD, blood oxygen level dependent.

near the recording site, as expected, at a lag of ~4 sec (Fig. 6). The voxels of the homologous region of cortex in the opposite hemisphere also exhibited higher correlation relative to other brain areas. The spatial correlation patterns indicate that the local but not global BOLD signals correlated to site-specific recordings, and the observation of correlation in contralateral SI supports a neural basis for the interhemispheric connectivity observed with fMRI.

Interhemispheric correlation of band-limited LFPs

BOLD fluctuations in left and right SI exhibit high correlation in both anesthetized rats and human subjects, making these areas an excellent network for investigating the neural basis of functional connectivity. Previous studies have shown that coherent band-limited LFPs are observed in bilateral sensory areas, which also exhibit strong functional connectivity in fMRI studies. For example, robust gamma power synchronization has been observed in the human auditory system in awake and sleeping subjects (Nir et al., 2008). In rats under alpha-chloralose anesthesia the strongest coherence in LFP power was observed in the delta band for the somatosensory system (Lu et al., 2007). In our study using isoflurane anesthesia, we also found synchronized interhemispheric LFP power fluctuations, but with synchronization in all frequency bands: delta (1–4 Hz), theta (4–8 Hz), alpha (8–14 Hz), low-beta (14–25 Hz), high-beta (25–40 Hz), and gamma (40–100 Hz). The synchrony in high-frequency bands (gamma/beta, 0.48 ± 0.15, mean ± STD) was significantly higher than that of low-frequency bands (theta/delta, 0.26 ± 0.13) ($p < 0.001$, Fig. 7). This synchronization across the spectrum may be attributed to bursting, which occurred at the same time in both hemispheres. During the suppression periods, on the other hand, there is little power in the LFP signals (Fig. 4).

Anesthesia-related changes in interhemispheric connectivity

Anesthesia effects on LFP coherence and functional connectivity were also examined in the present study. Significant changes in coherence as a function of anesthesia-related NSIs were found in the high- and low-frequency band LFP data ($p < 0.05$), but not in the middle-frequency bands (alpha). Interestingly, different dependencies on anesthesia were revealed for high- and low-frequency bands, with the coherent high-frequency bands (gamma/beta) showing an inverse relationship with NSI, whereas low-frequency bands (theta/delta) exhibited a positive relationship (Fig. 8). A significant

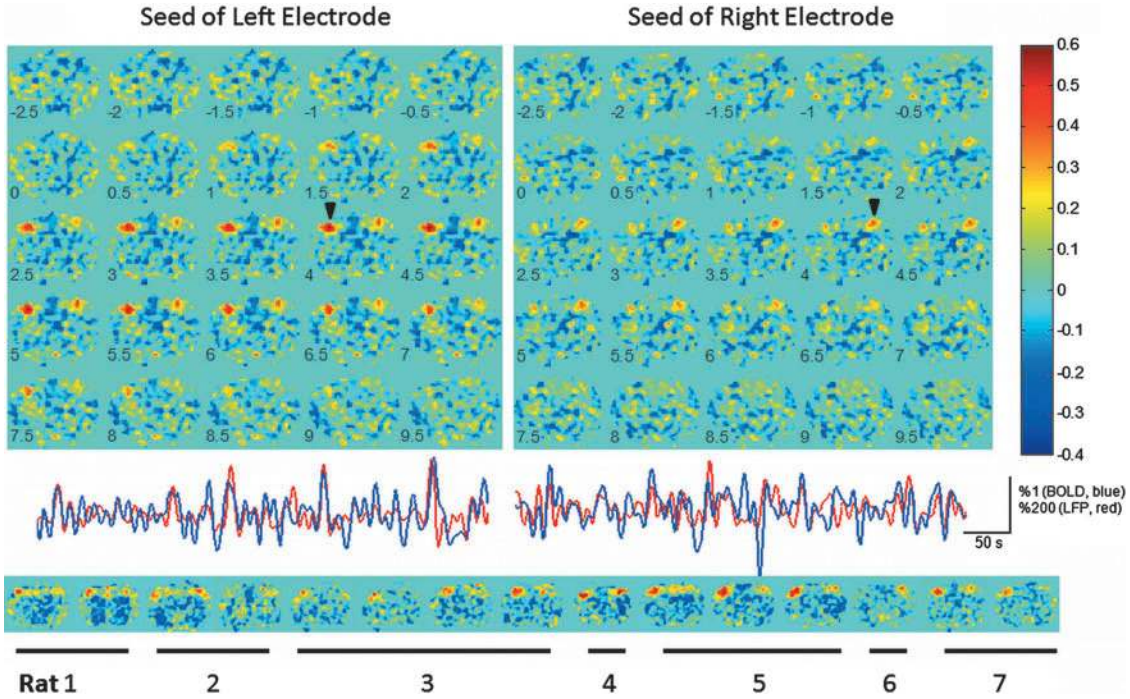

FIG. 6. Correlation analysis between power modulation of LFPs (1–100 Hz) and BOLD across a coronal image of the brain. The correlation is spatially restricted to the site of the microelectrode implantation (top panel, each arrow points to recording site with maximum correlation for each electrode; bottom panel, the individual correlation maps from left- or right-electrode recording for all 15 sessions from all 7 rats) and to SI in the contralateral hemisphere. The BOLD time lags are indicated at the left bottom corner of each map. The time courses of power fluctuations of broadband LFPs and 4-sec lagged BOLD (from the voxel with the highest correlation at the recording site) are shown in middle panel.

positive relationship between BOLD correlation and NSI was also observed, indicating that BOLD correlation follows the same trend as low-frequency LFP coherence. A direct comparison between BOLD correlation and band-limited LFP coherence showed that BOLD correlation was positively related with low-frequency LFP correlation (theta/delta, $p < 0.05$), but not with correlation in other frequency bands (gamma/beta/alpha) (Fig. 9).

Discussion

Relationship between spontaneous BOLD fluctuations and LFPs

Simultaneous fMRI and intracortical recording in the rat model revealed a close relationship between BOLD and broadband LFPs with direct spatial correspondence in the somatosensory cortex. The spatial distribution of correlations was estimated by computing correlation between the LFP power and BOLD fluctuations in a voxel-by-voxel fashion (Fig. 6). The strongest correlation was limited to small areas, located at the sites of the microelectrodes, a few voxels in size for most rats. The results are highly reproducible, with localized correlation observed in both hemispheres when either the ipsilateral or contralateral electrode was used as the seed.

Despite differences in measurement techniques, these results are in agreement with previous studies that showed a correlation between spontaneous neural activity and BOLD (Shmuel and Leopold, 2008) or cerebral blood flow (Golanov et al., 1994; Liu et al., 2011). Using concurrent blood flow/LFP recording, Martin et al. (2006) observed ~4 sec hemodynamic latency against neural response under anesthesia, similar to our findings that peak correlation between power modulation of broadband LFPs and low-frequency BOLD fluctuations occurs at a time lag of ~4 sec. An advantage of fMRI over Doppler blood flowmetry is that it can estimate not only temporal but also spatial relationships when correlated to LFPs, and demonstrates the local nature of the correlation between BOLD and neural activity. Similar work with fMRI by Shmuel and Leopold in monkeys found peak correlation between the signal from a single electrode and the BOLD signal at ~6 sec (Shmuel and Leopold, 2008), which probably reflects the difference between hemodynamic delays in monkeys as compared to rats. They also observed BOLD correlation that propagates away from the LFP recording electrode as a function of time lag (Shmuel and Leopold, 2008), which was not observed in this study. Interestingly, in a recent article by Schölvinck, the signal from a single electrode was shown to correlate with the BOLD signal from the entire brain (Schölvinck et al., 2010). This was not observed in our study even when global correction was not performed. Previous studies have also shown that global synchronizations in spontaneous activities are enhanced during the resting state (Vanderwolf, 1975). Synchronization of low-frequency activity in the cortex likely involves ascending modulation of the reticular-thalamus-neocortex, mediated by the basal forebrain system (Buzsaki et al., 1988). While the global fluctuations undoubtedly play an important role in brain function, locally correlated spontaneous activity may better reflect the local information transfer involved in specialized functions.

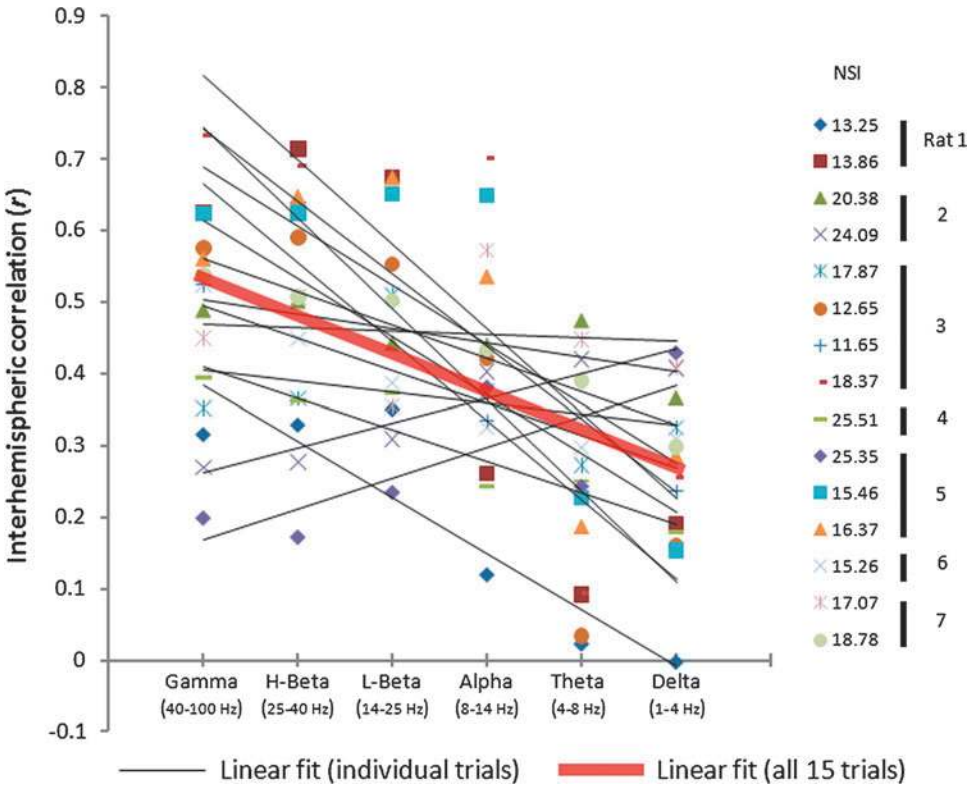

FIG. 7. Interhemispheric correlation in power modulation of LFPs across frequency bands. Despite differences in anesthesia levels across 15 study sessions, the pooled data showed a significant negative trend of interhemispheric coherence from high-frequency bands to low-frequency bands ($y = -0.0532x + 0.5819$, $R^2 = 0.273$, $p < 0.001$).

In the present findings, the highest correlation observed between the BOLD signal and the power modulation of LFP activity consistently occurred at a 4-sec time lag across all LFP broadband frequencies (1–300 Hz). In rat somatosensory cortex under anesthesia, we found the prominent frequency in recording data was <150 Hz oscillations, and the analysis included all frequency bands of LFPs (1–300). The power fluctuations in broadband LFPs may have particular importance. For example, recent studies revealed that broadband power shifts were a more reliable predictor of neuronal spiking than narrowband power shifts (Manning et al., 2009).

When the rat is anesthetized with isoflurane, spontaneous neural activity is typically observed as well-recognized burst-suppression patterns, and the local blood flow has been observed to faithfully follow the spontaneous neural bursts (Golanov et al., 1994), with the neurovascular coupling preserved on a fine temporal scale (Liu et al., 2011). Relative to these studies of cerebral blood flow (CBF) measured with Doppler flowmetry, fMRI BOLD signals tend to have a lower signal-to-noise ratio (SNR) (one order of magnitude less than CBF). Possibly due to the nature of fMRI SNR, we did not obtain the precise correspondences of fMRI BOLD profiles with electrical signals in a temporal scale as brief as seen in the CBF signal measured by laser-Doppler flowmetry (Golanov et al., 1994; Liu et al., 2011). Rather than short time scale analysis, we compared neural/BOLD fluctuations with a relative large time scale (<0.1 Hz), which are the dominant components in resting-state activity (Biswal et al., 1995). In this study, the significant correlations were revealed between the slow fluctuations of BOLD signals and LFP power, which is in agreement with recent simultaneous fMRI and electrophysiology studies (Shmuel and Leopold, 2008). These results suggest that the resting-state BOLD fMRI signals of low-frequency components may well reflect slow power modulation of LFPs during the resting state (with a temporal scale of <0.1 Hz).

Anesthesia effects on spontaneous fluctuations and connectivity

The present studies in the rat model were performed under anesthesia, unlike the vast majority of human functional connectivity studies. During anesthesia, neural activity, metabolism, and hemodynamics are altered. The exact changes depend on the type and dose of anesthetic agent employed. For instance, isoflurane induces a decrease in glucose utilization and an increase in blood flow throughout the brain (Lenz et al., 1998). The deep sleep-like states induced by isoflurane anesthesia typically result in slow wave field potential fluctuations and burst-suppression patterns of rhythmic neural bursts. In a study using a similar anesthetic agent in humans, cortical gamma activity in the medial temporal lobe was observed to be suppressed gradually as levels of sevoflurane were increased (Uchida et al., 2000). The anesthesia-induced hypnosis is related to thalamic deactivation and loss of thalamo-cortical connectivity, with observed frequency transition from alpha (7–14 Hz) to delta (1–4 Hz) (Franks, 2008; White and Alkire, 2003). This shift in activity from higher to lower frequencies may be reflected in the increased coherence we observed in the lower frequency bands as anesthesia level increased.

The effects of anesthesia on functional connectivity have been addressed previously by a few studies, including one on sevoflurane in humans (Peltier et al., 2005) and another using isoflurane in rats (Liu et al., 2011). Marked attenuation and even absence of functional connectivity during deep anesthesia were described in each of these studies. We performed experiments on several rats under high concentrations of

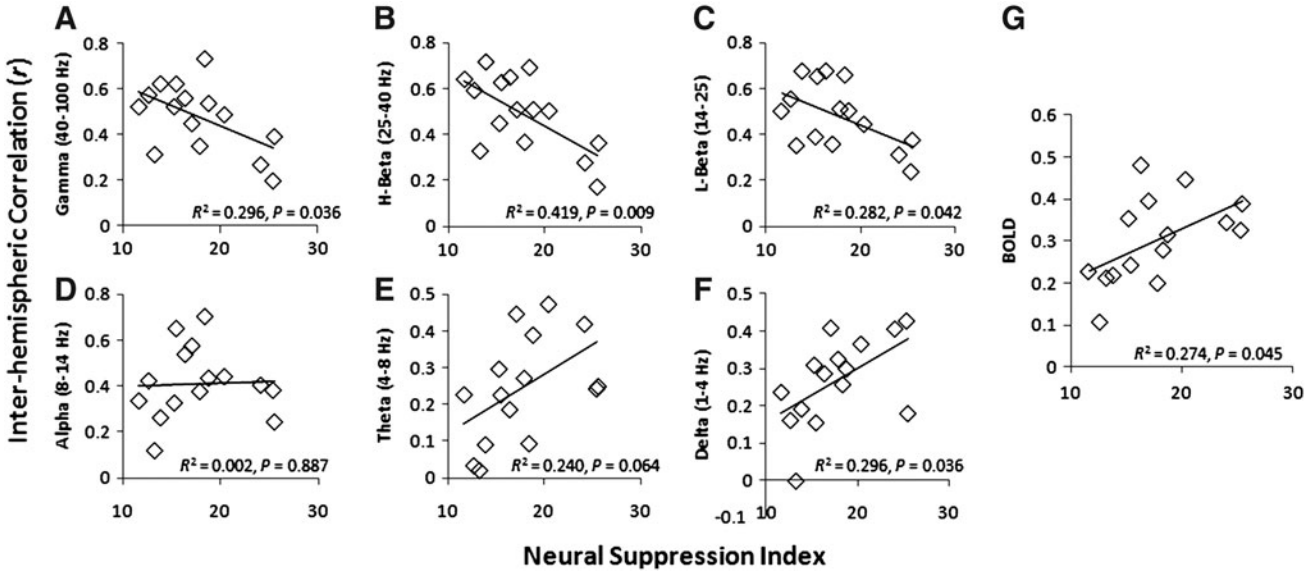

FIG. 8. Anesthesia modulation of interhemispheric correlations. The neural suppression induced by 1%–1.8% isoflurane was quantified as neural suppression index (NSI) for each session. The pooled data (15 sessions) show that the high- and low-frequency bands are significantly correlated with NSI, but with different trends: negative for gamma/beta **(A–C)**, but positive for theta/delta **(E** and **F)**. No correlation was observed for the alpha band **(D)**. The BOLD **(G)** was in line with theta/delta in response to anesthesia effects.

isoflurane (>2%, not shown) and found an absence of interhemispheric BOLD connectivity, although coherent electrical fluctuations were preserved. This observation is in line with previous reports of deep anesthesia (Liu et al., 2011). To examine the relationship between BOLD and LFPs, we focused on a range of anesthesia levels (1%–1.8% isoflurane), which is lighter than the dose used by the previous reports (Liu et al., 2011). Further, we utilized the inter-burst intervals, quantified by NSI, to describe the actual level of neural activity, which allows finer discrimination of anesthesia effects. Interestingly, while increasing the level of isoflurane from 1% to 1.8%, correlated BOLD fluctuations between hemispheres as well as coherent theta/delta LFP power fluctuations increased significantly. On the contrary, the higher coherence originally observed in the gamma/beta band decreased gradually with increased isoflurane levels. These findings are in line with recent studies

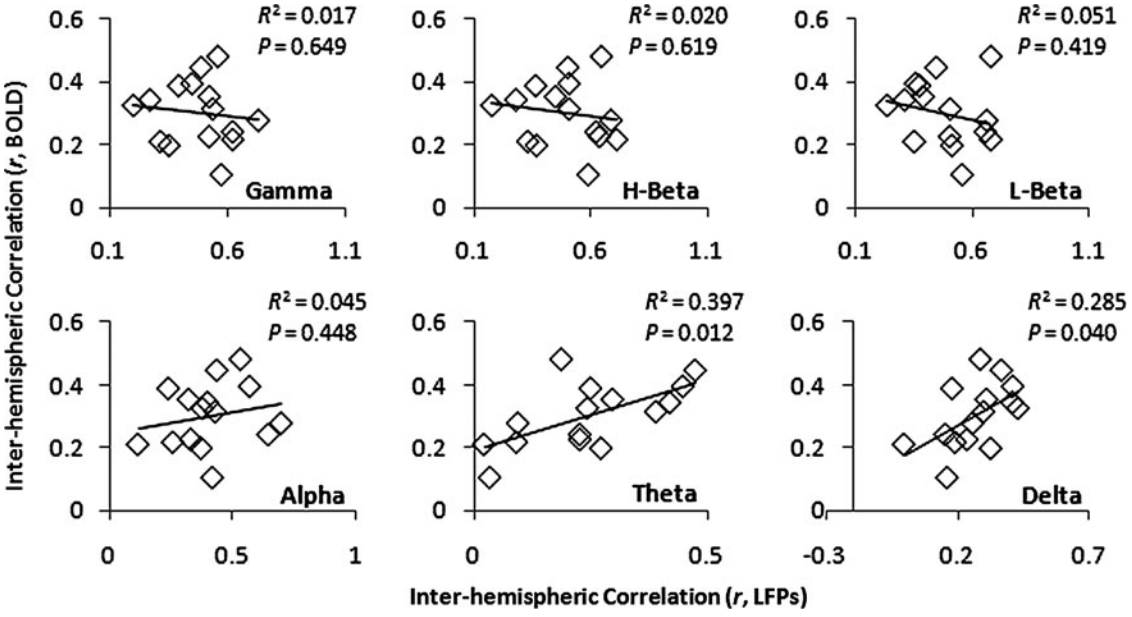

FIG. 9. Direct comparison between interhemispheric BOLD correlation and interhemispheric correlation in different bands of LFP. The pooled data (15 sessions) show that interhemispheric correlation in the BOLD signal behaved similarly to interhemispheric correlation in the low-frequency bands of LFPs (theta/delta) when modulated by levels of anesthesia.

showing in humans that the slow cortical potentials (<4 Hz) recorded by ECoG demonstrate a correlation structure similar to that of spontaneous BOLD fluctuations across wakefulness, slow-wave sleep, and rapid-eye-movement sleep (He et al., 2008). In contrast, gamma frequency power modulation also showed similar correlation structure but only during wakefulness and rapid-eye-movement sleep. Our findings are also in agreement with previous alpha-chloralose anesthetized rat results: striking interhemispheric correlations between delta-band power fluctuations (Lu et al., 2007). The anesthetized state may be closer to slow-wave sleep than REM sleep or wakefulness, as similar connectivity patterns were determined between BOLD and low-frequency LFP bands but not higher frequency bands.

However, the bursts of activity interleaved with prolonged silent periods typically observed under isoflurane anesthesia are very different than the continuous activity seen in awake human subjects, and caution should be used in extrapolating from the results of these experiments. In particular, the presence of bursts guarantees a broad range of frequency content in the LFP signal and may lead to more broadband correlation than would be observed in awake subjects. Nevertheless, the correlation between BOLD and LFP is localized to homologous areas of the two hemispheres, suggesting that if bursts are a major contributor to the LFP power, they are relatively localized and coordinated across hemispheres. The results of this study provide insight into the wide body of brain research performed in the isoflurane-anesthetized rodent, and further work will extend these experiments to other anesthetics with different effects on neural activity to determine whether broadband correlation is still present.

An alternative explanation that deserves consideration is that the isoflurane-induced vasodilation affects the coherence of the oscillations. While cerebral blood flow was not measured in this study, previous work suggests that an increase of 20%–30% should accompany a change in isoflurane level from 0.5 MAC to 1.5 MAC (Lee et al., 1995). It is possible that the change in vascular tone increases the amplitude of the fluctuations compared to baseline and thus correlation in the BOLD signal increases as anesthesia deepens, independent of the coherence in neural activity. However, previous studies where hypercapnia was administered to increase cerebral blood flow actually demonstrate a reduction of BOLD fluctuations in the lowest frequencies (Biswal et al., 1997), and an additional analysis of our data (not shown) found no significant relationship between low-frequency BOLD power and NSI. Also, our work agrees with a previous experiment in which Lu et al. indirectly demonstrated a relationship between low-frequency electrical activity and BOLD correlation under increasing doses of alpha-chloralose, an injectable anesthetic that lacks the strong vasoactive properties of isoflurane. While this suggests that the BOLD correlations are likely to be related to low-frequency coherence in the isoflurane-anesthetized rat, further work that examines the effect of the anesthetic directly on the vasculature is needed before stronger conclusions can be drawn.

Technical considerations for simultaneous fMRI and intracortical recordings

To adapt classical intracortical electrophysiology techniques to recording in the MRI scanner, the recording cables were extended to ~5 m long to reach outside of the magnet room, but no obvious voltage loss relative to 1.5-m-cable bench-top recordings was observed. The MRI scanner room is contained within a high-quality Faraday cage, which reduces environmental noises picked up from input cables.

The modified surgery paradigm for electrode implantation was designed to minimize the potential interferences on MRI EPI imaging due to surgery. Efforts were adopted to avoid any possible susceptibility mismatches within imaging regions, including replacement of removed scalp with toothpaste that matched the signal intensity of the removed tissue. The electrodes were obliquely inserted to avoid the inclusion of electrode shafts in the image region. Although the glass microelectrode is nonmagnetic, the water-based electrode solution in the shafts caused MRI artifacts along the shaft direction that interfered with the brain image when the shaft was included in the image slice. The dental cement fixation point was placed far away from the imaging area, because the cement has low MRI signal that caused sharp contrast on the brain surface and resulted in image artifacts.

One limitation of the simultaneous imaging and recording approach developed for this study is that the ideal area for image acquisition is small (the slice containing the electrodes and potentially 1–2 anterior slices). The caudal slices are disturbed by the passage of the electrodes. The challenges of combined recording and imaging experiments grow as the number of electrodes is increased, due to the complexity of the preparation. Eventually, we hope to record from multiple cortical and subcortical sites while imaging, allowing a more thorough investigation into the neural underpinnings of BOLD correlation than our current study, which was limited to a single network.

To our knowledge, this is the first study combining simultaneous extracellular recording from two cortical areas with fMRI data acquisition, allowing a direct comparison between the relationship between the BOLD signal from the two sites and the electrical signal from the two sites. In addition, we were first to introduce glass microelectrodes into simultaneous fMRI/recording study (Pan et al., 2010). In contrast to other MRI-compatible electrodes including metal wire and carbon fiber, the present procedure with glass capillary implantation will allow extending the simultaneous study to include microinjection in the future.

Several possibilities have been suggested for the functional role of the correlated spontaneous fluctuations, such as memory maintenance (Stickgold et al., 2001), renormalization of synaptic contacts (Tononi and Cirelli, 2006), and preparation for rapid inputs by balanced spontaneous excitation/inhibition activity (Vogels et al., 2005). These functions could all contribute to the functional connectivity measured with BOLD, and further studies in the rodent model may elucidate the mechanisms that lead to BOLD correlations.

Conclusions

In summary, the present study demonstrates for the first time the use of simultaneous multi-site intracortical recording and fMRI in the rat model and provides an insight into the neural basis of the spontaneous BOLD signal and connectivity. The observed tight coupling between temporal and spatial measures provides evidence of a neural correlate of BOLD fluctuations. BOLD, with a ~4 sec time lag, registered

to broadband LFPs with spatial restriction to the recording site and contralateral site in the other hemisphere. These findings demonstrated that all frequency bands of LFPs have significant correlations with spontaneous BOLD fluctuations, which suggests that broadband LFPs contribute to the neural origin of the resting-state fMRI BOLD signal at least in the isoflurane-anesthetized rat. The bi-hemispheric recording and simultaneous fMRI imaging allow direct comparison of the interhemispheric connectivity between BOLD and neural electrical activity. This work provides an experimental model for combined multi-site electrophysiology and fMRI in the rodent.

Acknowledgment

The work was supported by NIH R21NS057718-01.

Author Disclosure Statement

No competing financial interests exist.

References

Allen PJ, Josephs O, Turner R. 2000. A method for removing imaging artifact from continuous EEG recorded during functional MRI. Neuroimage 12:230–239.

Biswal B, Hudetz AG, Yetkin FZ, Haughton VM, Hyde JS. 1997. Hypercapnia reversibly suppresses low-frequency fluctuations in the human motor cortex during rest using echo-planar MRI. J Cereb Blood Flow Metab 17:301–308.

Biswal B, Yetkin FZ, Haughton VM, Hyde JS. 1995. Functional connectivity in the motor cortex of resting human brain using echo-planar MRI. Magn Reson Med 34:537–541.

Buzsaki G, Bickford RG, Ponomareff G, Thal LJ, Mandel R, Gage FH. 1988. Nucleus basalis and thalamic control of neocortical activity in the freely moving rat. J Neurosci 8:4007–4026.

Fox MD, Raichle ME. 2007. Spontaneous fluctuations in brain activity observed with functional magnetic resonance imaging. Nat Rev Neurosci 8:700–711.

Franks NP. 2008. General anaesthesia: from molecular targets to neuronal pathways of sleep and arousal. Nat Rev Neurosci 9:370–386.

Goense JB, Logothetis NK. 2008. Neurophysiology of the BOLD fMRI signal in awake monkeys. Curr Biol 18:631–640.

Golanov EV, Yamamoto S, Reis DJ. 1994. Spontaneous waves of cerebral blood flow associated with a pattern of electrocortical activity. Am J Physiol 266:R204–R214.

Gruetter R. 1993. Automatic, localized *in vivo* adjustment of all first- and second-order shim coils. Magn Reson Med 29: 804–811.

He BJ, Snyder AZ, Zempel JM, Smyth MD, Raichle ME. 2008. Electrophysiological correlates of the brain's intrinsic large-scale functional architecture. Proc Natl Acad Sci U S A 105: 16039–16044.

Huttunen JK, Grohn O, Penttonen M. 2008. Coupling between simultaneously recorded BOLD response and neuronal activity in the rat somatosensory cortex. Neuroimage 39:775–785.

Lee JG, Smith JJ, Hudetz AG, Hillard CJ, Bosnjak ZJ, Kampine JP. 1995. Laser-Doppler measurement of the effects of halothane and isoflurane on the cerebrovascular CO2 response in the rat. Anesth Analg 80:696–702.

Lenz C, Rebel A, van Ackern K, Kuschinsky W, Waschke KF. 1998. Local cerebral blood flow, local cerebral glucose utilization, and flow-metabolism coupling during sevoflurane versus isoflurane anesthesia in rats. Anesthesiology 89:1480–1488.

Lewin JS, Wu D, Durek JL. 1995. Susceptibility-induced artifacts in functional Mr-imaging. Radiology 197:219–219.

Liu X, Zhu XH, Zhang Y, Chen W. 2011. Neural origin of spontaneous hemodynamic fluctuations in rats under burst-suppression anesthesia condition. Cereb Cortex 21:374–384.

Logothetis NK. 2008. What we can do and what we cannot do with fMRI. Nature 453:869–878.

Logothetis NK, Murayama Y, Augath M, Steffen T, Werner J, Oeltermann A. 2009. How not to study spontaneous activity. Neuroimage 45:1080–1089.

Logothetis NK, Pauls J, Augath M, Trinath T, Oeltermann A. 2001. Neurophysiological investigation of the basis of the fMRI signal. Nature 412:150–157.

Lu H, Zuo Y, Gu H, Waltz JA, Zhan W, Scholl CA, et al. 2007. Synchronized delta oscillations correlate with the resting-state functional MRI signal. Proc Natl Acad Sci U S A 104: 18265–18269.

Manning JR, Jacobs J, Fried I, Kahana MJ. 2009. Broadband shifts in local field potential power spectra are correlated with single-neuron spiking in humans. J Neurosci 29:13613–13620.

Martin C, Martindale J, Berwick J, Mayhew J. 2006. Investigating neural-hemodynamic coupling and the hemodynamic response function in the awake rat. Neuroimage 32:33–48.

Nir Y, Mukamel R, Dinstein I, Privman E, Harel M, Fisch L, et al. 2008. Interhemispheric correlations of slow spontaneous neuronal fluctuations revealed in human sensory cortex. Nat Neurosci 11:1100–1108.

Pan WJ, Thompson G, Magnuson M, Majeed W, Jaeger D, Keilholz S. 2010. Simultaneous FMRI and electrophysiology in the rodent brain. J Vis Exp. (42):pii:1901.

Peltier SJ, Kerssens C, Hamann SB, Sebel PS, Byas-Smith M, Hu X. 2005. Functional connectivity changes with concentration of sevoflurane anesthesia. Neuroreport 16:285–288.

Schölvinck ML, Maier A, Ye FQ, Duyn JH, Leopold DA. 2010. Neural basis of global resting-state fMRI activity. Proc Natl Acad Sci U S A 107:10238–10243.

Shmuel A, Leopold DA. 2008. Neuronal correlates of spontaneous fluctuations in fMRI signals in monkey visual cortex: Implications for functional connectivity at rest. Hum Brain Mapp 29:751–761.

Stickgold R, Hobson JA, Fosse R, Fosse M. 2001. Sleep, learning, and dreams: off-line memory reprocessing. Science 294:1052–1057.

Tononi G, Cirelli C. 2006. Sleep function and synaptic homeostasis. Sleep Med Rev 10:49–62.

Uchida S, Nakayama H, Maehara T, Hirai N, Arakaki H, Nakamura M, et al. 2000. Suppression of gamma activity in the human medial temporal lobe by sevoflurane anesthesia. Neuroreport 11:39–42.

Vanderwolf CH. 1975. Neocortical and hippocampal activation relation to behavior: effects of atropine, eserine, phenothiazines, and amphetamine. J Comp Physiol Psychol 88: 300–323.

Vincent JL, Patel GH, Fox MD, Snyder AZ, Baker JT, Van Essen DC, et al. 2007. Intrinsic functional architecture in the anaesthetized monkey brain. Nature 447:83–86.

Viswanathan A, Freeman RD. 2007. Neurometabolic coupling in cerebral cortex reflects synaptic more than spiking activity. Nat Neurosci 10:1308–1312.

Vogels TP, Rajan K, Abbott LF. 2005. Neural network dynamics. Annu Rev Neurosci 28:357–376.

White NS, Alkire MT. 2003. Impaired thalamocortical connectivity in humans during general-anesthetic-induced unconsciousness. Neuroimage 19:402–411.

Williams KA, Magnuson M, Majeed W, LaConte SM, Peltier SJ, Hu X, et al. 2010. Comparison of alpha-chloralose, medetomidine and isoflurane anesthesia for functional connectivity mapping in the rat. Magn Reson Imaging 28: 995–1003.

Address correspondence to:
Shella Keilholz
Department of Biomedical Engineering
Emory University/Georgia Institute of Technology
101 Woodruff Circle, Suite 2001
Atlanta, GA 30322

E-mail: shella.keilholz@bme.gatech.edu